Ligand Binding Modulates the Mechanical Stability of Dihydrofolate Reductase

Sri Rama Koti Ainavarapu, Lewyn Li, Carmen L. Badilla, and Julio M. Fernandez
Department of Biological Sciences, Columbia University, New York, New York

ABSTRACT We use single-molecule force spectroscopy to demonstrate that the mechanical stability of the enzyme dihydrofolate reductase (DHFR) is modulated by ligand binding. In the absence of bound ligands, DHFR extends at very low forces, averaging 27 pN, without any characteristic mechanical fingerprint. By contrast, in the presence of micromolar concentrations of the ligands methotrexate, nicotinamide adenine dihydrogen phosphate, or dihydrofolate, much higher forces are required (82 ± 18 pN, 98 ± 15 pN, and 83 ± 16 pN, respectively) and a characteristic fingerprint is observed in the force-extension curves. The increased mechanical stability triggered by these ligands is not additive. Our results explain the large reduction in the degradation rate of DHFR, in the presence of its ligands. Our observations support the view that the rate-limiting step in protein degradation by adenosine triphosphate-dependent proteases is the mechanical unfolding of the target protein.

INTRODUCTION

Dihydrofolate reductase (DHFR) is an essential enzyme that converts 7,8-dihydrofolate (DHF) to 5,6,7,8, tetrahydrofolate (THF) in the presence of nicotinamide adenine dihydrogen phosphate (NADPH) (1,2). THF serves as the vital one-carbon donor in the syntheses of thymidylate and purine nucleosides. Inhibiting DHFR blocks DNA synthesis and kills the cell. Anti-folate drugs such as methotrexate (MTX), which bind to DHFR more strongly than the natural substrate DHF, are common cancer therapeutics (3). The binding sites of NADPH and DHF/MTX are located in two different regions of DHFR, but, at the enzyme's active site, the two ligands come into close proximity to enable hydride transfer from NADPH to DHF (4).

Ligand-binding-induced conformational changes in proteins are ubiquitous (5–8). Structural changes accompanied by ligand binding are important in the enzymatic function of GTP-binding proteins (5), ion channels (6), and calcium binding proteins (7,8) to name a few. Ligand binding also affects the thermodynamic stability of proteins (7,8). Ligand binding to DHFR also causes large changes in thermodynamic stability (9). The midpoint urea-induced unfolding transition of human DHFR is shifted from 1.4 M urea to 2.8 M urea in the presence of $NADP^+$/folate (9).

The large changes in thermodynamic stability induced by the binding of MTX have made DHFR the molecule of choice in studying protein translocation through protein channels like those of the mitochondrial membrane (10,11) as well as those of the adenosine triphosphate (ATP)-dependent proteases found in prokaryotes and eukaryotes (12,13). These channel pores are narrow, ranging between 10–22 Å (14–16). Hence, folded globular proteins, ranging in size upwards from ~5 nm, must be unfolded before they can enter the protein channels of the mitochondrial membrane import motor (11,17) and ATP-dependent proteases (17–20). Various studies have proposed that the mitochondrial import motors (Hsp70) are capable of doing mechanical work either as a Brownian ratchet (16), or as molecular motors (21) or ratchet-motor mixtures (22). These publications suggest that mechanical unfolding of the targeted protein is an essential step in translocation through protein channels. DHFR has played a significant role in these studies. In the absence of MTX, DHFR readily traverses the translocation protein channels in mitochondria (10,11) and the degradation protein channel in the proteasome (12,23), whereas addition of MTX pronouncedly slows the rate of both the mitochondrial import (10,11) and the proteasomal degradation of DHFR (12,23). These observations suggest that MTX increases the mechanical stability of DHFR. In this article, we used protein engineering combined with single-molecule atomic force microscopy (AFM) techniques (24–29) to test this hypothesis.

A detailed sequence of events taking place in a typical polyprotein stretching experiment by single-molecule atomic force microscopy is depicted in Fig. 1 *A* and the resulting sawtooth pattern force-extension curve in Fig. 1 *B*. The mechanical stability of the protein being measured can be readily determined from the average peak force required to unfold each module (28).

Our experimental results demonstrate that DHFR unravels easily at forces averaging 27 pN, and binding ligands or inhibitor increases its unfolding force to 83 pN. The increased mechanical stability directly explains the large reduction in the degradation rate of DHFR when bound to one of its ligands (12,23), supporting the view that mechanical unfolding is a required step before protein translocation or degradation (23,30). Our study is the first demonstration that ligand binding can strengthen a protein against mechanical stress. Together with the recent discovery that the

Submitted February 28, 2005, and accepted for publication August 1, 2005.
Sri Rama Koti Ainavarapu and Lewyn Li contributed equally to this work.
Address reprint requests to J. M. Fernandez, Tel.: 212-854-9141; E-mail: jfernandez@columbia.edu.

0006-3495/05/11/3337/08 $2.00
doi: 10.1529/biophysj.105.062034

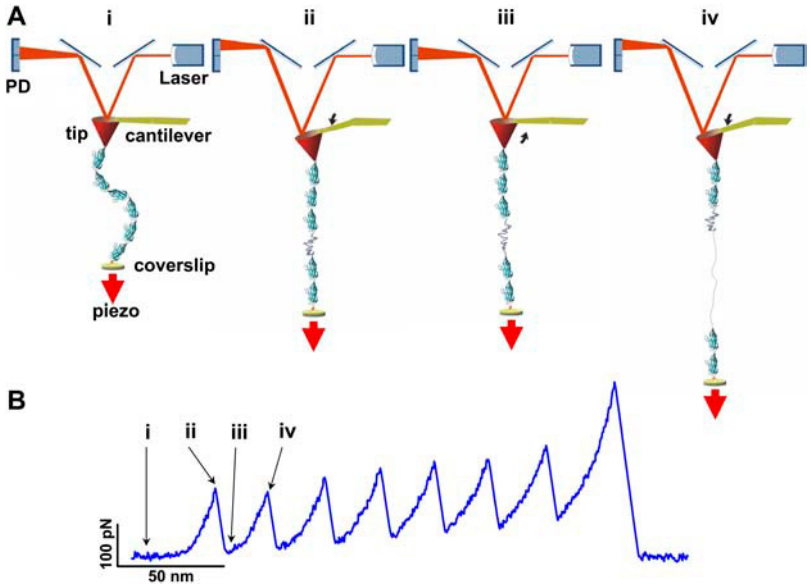

FIGURE 1 Mechanical stretching of a polyprotein using single-molecule atomic force microscopy. (*A*) (*i*) A single polyprotein molecule is held between the cantilever tip and the coverslip, whose position can be controlled with high precision using a piezoelectric positioner (*piezo*). (*ii*) Moving the coverslip away from the tip exerts a stretching force on the polyprotein, which in turn bends the cantilever. The bending of the cantilever changes the position of the laser beam on the split photo diode (*PD*), registering the pulling force. The applied force can be determined from the spring constant of the cantilever and the degree of cantilever bending. At this high pulling force, a protein domain unfolds. (*iii*) The unfolded domain can now readily extend, relaxing the cantilever. (*iv*) The piezo continues to move, stretching the polyprotein to a new high force peak, repeating the sequence until the whole polyprotein has unfolded. This process results in a force-extension curve with a characteristic sawtooth pattern shape. (*B*) A typical sawtooth pattern curve obtained by stretching an $I27_8$ polyprotein (28). The labels *i–iv* represent the sequence of events shown in *A*.

mechanical stability of a protein depends on the direction of the applied force (31,32), ligand modulation of mechanical stability as reported here opens a previously unrecognized perspective in cell biology.

METHODS

Protein engineering

$(DHFR)_8$ and $(I27\text{-}DHFR)_4$ were constructed following the methods described previously (29). Briefly, the Chinese hamster ovary DHFR (CHO-DHFR) gene, which is ≈90% homologous to the human gene, was amplified by PCR with 5′ *Bam*HI restriction site and 3′ *Bgl*II and *Kpn*I restriction site and cloned into the vector pT7Blue (Novagen, Madison, WI). In the case of the $(I27\text{-}DHFR)_4$, we used the vector pT7Blue, which already contained the clone of human cardiac immunoglobulin I27 (24). Iterative cloning was used to make the synthetic genes of $(I27\text{-}DHFR)_4$ and $(DHFR)_8$. These genes were cloned into the expression vector pQE16 (Qiagen, Hilden, Germany). Protein expression was done in BLR(DE3) cells (Novagen) in the presence of 1 mM IPTG. The proteins were purified with Ni^{2+} affinity chromatography and eluted with a buffer (pH 7.0) containing 250 mM imidazole, 50 mM sodium phosphate, and 300 mM sodium chloride.

Chemicals

MTX, NADPH, and DHF were purchased from Sigma-Aldrich (St. Louis, MO) and used without further purification. Phosphate-buffered saline (PBS) was used for making stock solutions. MTX was first dissolved in a minimum amount of 0.1 N NaOH and then diluted to the desired concentration with PBS buffer. The pH of the resulting solution was adjusted to 7.4.

Single-molecule AFM experiment

The details of the atomic force microscope and its mode of operation have been described elsewhere (33). The spring constant of the cantilevers that we used was ≈40 pN/nm, measured using the equipartition theorem (34). Unless stated otherwise, we used a pulling rate of 400 nm/s and the peak-to-peak noise in the recordings was 15 ± 4 pN.

RESULTS

The DHFR-MTX complex is mechanically stable

To examine the mechanical stability of DHFR we used protein-engineering techniques to construct a polyprotein (35) made of eight identical repeats of DHFR (see Methods, above). We use polyproteins to identify the molecule being pulled by the AFM. Polyproteins give a characteristic sawtooth pattern in the force-extension curves, serving as a fingerprint to identify the molecule that is being pulled. This is essential given that a majority of the force-extension curves arise from pulling unidentified molecules and only 1–10% of the pulls result in sawtooth patterns (36). Despite these considerations, force-extension curves obtained by stretching the $DHFR_8$ polyprotein were featureless and never showed the characteristics of a sawtooth pattern (regularly spaced peaks of similar amplitude). These data could be interpreted as an indication that the DHFR protein lacks mechanical stability. However, the data show a negative result and therefore we cannot be certain whether DHFR is mechanically unstable, or we simply failed to correctly pick up the native form of the protein (Fig. 2 *A*). A very different result was observed when we added 1.2 mM MTX to the bathing solution. Under these conditions we repeatedly observed force-extension curves displaying sawtooth patterns with peak unfolding forces averaging 78 ± 14 pN (n = 72) (Fig. 2 *B*; see also Table 1). The increase in contour length of the unfolding molecule was determined by fitting the wormlike chain (WLC) model of polymer elasticity to the segment of the force-extension curve leading up to each peak (Fig. 2 *B*; *thin lines*). We measured a spacing between peaks of 67.3 ± 0.5 nm (n = 72). This contour length increment is in close agreement with an expected value of ~65 nm, calculated from the number of amino acids in the DHFR

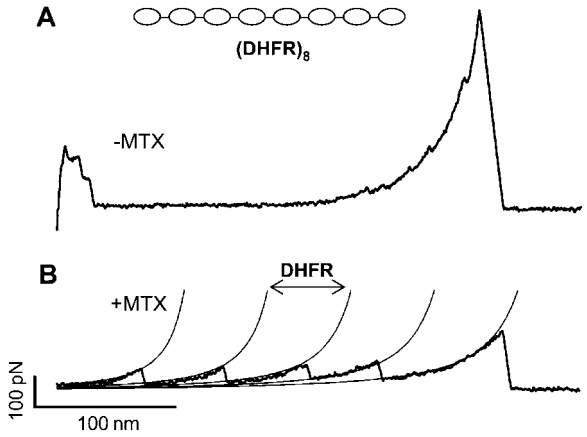

FIGURE 2 The force necessary to unfold DHFR is dependent on the presence of the ligand Methotrexate (MTX). (*A*) Force-extension curve obtained by stretching the polyprotein $DHFR_8$ in the absence of methotrexate (MTX). The lack of a sawtooth pattern suggests that DHFR is mechanically weak. However, absence of a fingerprint makes it difficult to be certain that such recordings correspond to DHFR and not from a contaminating molecule. (*B*) Force-extension curve obtained by stretching the polyprotein $DHFR_8$ in the presence of 1.2 mM MTX. We now observe a force-extension curve showing a clear sawtooth pattern of unfolding events at an average force of 78 pN ± 14 ($n = 72$; see Table 1). Fits of the wormlike chain (WLC) model of polymer elasticity (*thin lines*) reveal a contour increment between unfolding events of $\Delta L_c = 67.3 \pm 0.5$ nm ($n = 72$), which is in close agreement with the expected length gained by unfolding a DHFR molecule (65 nm).

sequence (186 aa × 0.36 nm/aa = 67 nm) minus the end-to-end distance of the folded DHFR protein (1.8 nm for Human DHFR).

It was clear from the experiments that the $DHFR_8$ polyprotein could not be used if the protein became mechanically weak in the absence of the MTX ligand. Under those conditions, the lack of a clear fingerprint prevented us from positively identifying the molecules being pulled. Hence, we engineered protein chimeras where DHFR was combined with an immunoglobulin-like module (I27 from human cardiac titin) that would provide a clear sawtooth pattern fingerprint even when MTX was absent (29,37). Accordingly, we constructed a $(DHFR\text{-}I27)_4$ polyprotein. The I27 protein module serves as fingerprint with a regular spacing of 28.1 nm and an unfolding force of ~200 pN (29,35).

We started by stretching the $(DHFR\text{-}I27)_4$ polyprotein chimera, in a PBS solution containing 190 μM MTX. The resulting force-extension curves showed sawtooth patterns that contained two distinct regions (Fig. 3 *A*). The earliest region contained unfolding peaks of 82 ± 18 pN ($n = 277$; Fig. 3 *B*), which were equally spaced by contour length increments of 67.4 ± 1.0 nm ($n = 277$; Fig. 3 *C*) closely corresponding to the sawtooth patterns observed for the unfolding of the $DHFR_8$ polyprotein (Fig. 2 *B*). The later part of the sawtooth pattern was clearly marked by unfolding peaks of 220 ± 36 pN ($n = 322$), which were equally spaced with contour length increments of 28.0 ± 0.7 nm ($n = 322$), identifying them as I27 unfolding events (29,35). In the force-extension recordings of Fig. 3 *A*, we can clearly distinguish three or four I27 unfolding events, establishing unambiguously that the three earlier peaks arise from the unfolding of DHFR (see (29) for a discussion on the usage of the chimera approach). It is clear from the experiments that DHFR in the presence of MTX requires 78–82 pN to unfold.

TABLE 1 Mechanical properties of $(DHFR)_8$ under various conditions

	F_u (DHFR) pN	ΔL_c (DHFR) nm	n
1.2 mM MTX	78 ± 14	67.3 ± 0.5	72
190 μM MTX 210 μM NADPH	89 ± 17	62.8 ± 6.2	28

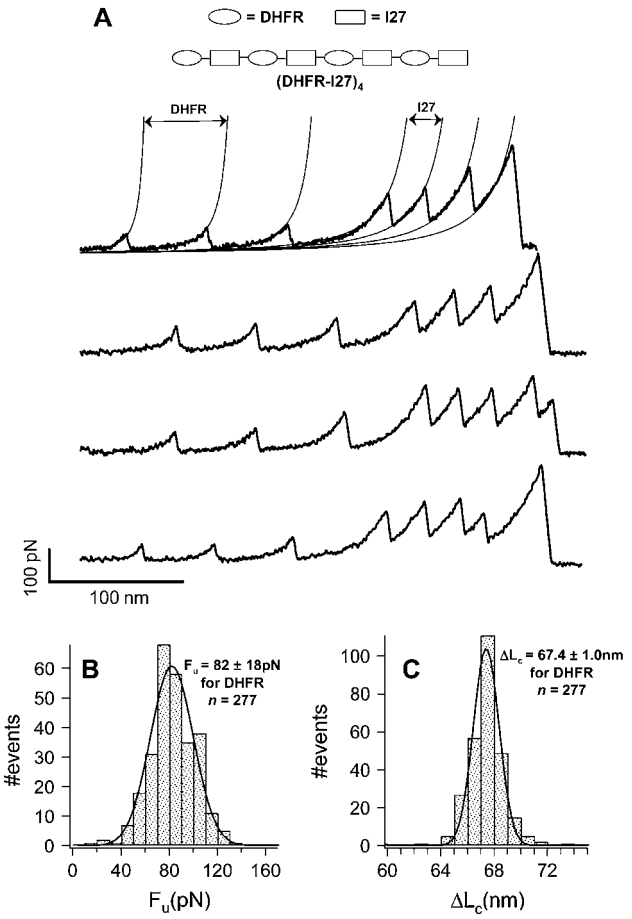

FIGURE 3 Use of a polyprotein chimera to probe the mechanical stability of DHFR. (*A*) A panel of four force-extension curves obtained by stretching the $(DHFR\text{-}I27)_4$ polyprotein chimera, in the presence of 190 μM MTX. The low unfolding force and much larger contour length easily distinguish the DHFR unfolding events (first) from the I27 unfolding events (last). Fits of the WLC model (*thin lines*) to the data are used to measure the contour length increment between unfolding events. (*B*) Histogram of unfolding forces for the DHFR-MTX complex. A Gaussian fit (*thin line*) gives 82 ± 18 pN ($n = 277$). (*C*) Histogram of contour length increments measured with the WLC. A Gaussian fit (*thin line*) gives 67.4 ± 1.0 nm ($n = 277$). By contrast, the unfolding force measured from the I27 peaks is 220 ± 36 pN and the contour length increment is 28.0 ± 0.7 nm ($n = 322$).

This unfolding force was found to be relatively independent of the MTX concentration in the range between 19 μM and 1.2 mM MTX (Table 2). We have done experiments at a lower pulling speed (80 nm/s) on (DHFR-I27)$_4$ in the presence of 190 μM MTX. At 80 nm/s, the DHFR unfolding force was 62 $\pm$ 7 pN. Under the same conditions the unfolding force for the I27 was 181 $\pm$ 24 pN, in close agreement with earlier results (28).

DHFR is mechanically weak

Force-extension curves obtained by stretching the (I27-DHFR)$_4$ polyprotein in the absence of any ligand are shown in Fig. 4 *A*. In contrast to the recordings obtained with MTX, the force-extension curves now show a featureless spacer followed by a set of I27 unfolding events. The I27 unfolding events are recognized by their characteristic unfolding force and contour length increment between peaks (209 $\pm$ 34 pN and 28.1 $\pm$ 1.3 nm, respectively; $n = 226$). The top two traces shown in Fig. 4 *A* show four I27 unfolding events implying that at least three DHFR molecules must have been stretched. In the bottom two traces showing three I27 unfolding events, we must have extended at least two DHFR proteins (see (29) for a discussion of this point). Most of the recordings obtained without MTX show similar results with only a long featureless spacer before the I27 fingerprint. However, in some cases, we observed either a sawtooth pattern at very low force (e.g., Fig. 4 *A*; *second trace* from the *top*) or isolated peaks in the region of the extension that should contain DHFR unfolding events. To estimate the force required to unfold DHFR in the absence of MTX, we constructed a series of WLC curves with contour length increments of $\Delta L_c = 67$ nm that end with the first I27 unfolding event (*dotted lines* in Fig. 4 *A*). The number of WLC curves was set to the minimum number of DHFR unfolding events expected for a given number of I27 unfolding events (see above). The highest force at which the WLC curves intersected the experimental trace was taken as the unfolding force of DHFR. A histogram ($n = 163$) of unfolding forces of DHFR is shown in Fig. 4 *B*, with a mean unfolding force of 27 pN, which is <50% of the force for the DHFR-MTX complex and it is close to the resolution of our apparatus (see Methods, above). Even at a higher pulling rate (4000 nm/s) we did not observe a mechanical fingerprint for DHFR. The force-extension curves obtained at 400 nm/s and 4000 nm/s were similar. The putative unfolding force of DHFR was higher at 4000 nm/s than at 400 nm/s (53 vs. 27 pN). Although the putative unfolding force doubled at 4000 nm/s, the peak-to-peak noise tripled on increasing the pulling speed (from 15 $\pm$ 4 pN to 48 $\pm$ 12 pN). At 4000 nm/s, 60% of the putative unfolding events occurred within the noise level (<50 pN) and the unfolding force histogram showed no clear feature above the noise level. Hence, the observed difference may not be significant. By contrast, we observed a clear difference in the unfolding force of the I27 module, which was found to be 262 $\pm$ 55 pN, in close agreement with those previously reported (28). Hence, when there is no ligand, DHFR does not show a significant mechanical stability. This is not surprising, given that there are proteins, with a well-defined folded structure, which were nonetheless shown not to have a measurable mechanical stability. For example, both calmodulin and barnase polyproteins were shown to extend readily at a low force without any unfolding force peaks (25,38). In both of these cases, the engineered polyproteins were shown to have a thermodynamic stability that was similar to that of the monomers (21,25,38). We have not measured the thermodynamic stability of the DHFR polyproteins due to the difficulty in expressing them in sufficiently large amounts for bulk experiments. However, the DHFR protein has been used extensively as a fusion protein with a variety of other proteins and peptides, without altering the stability of the protein (12,21,22,30,39,40).

The cumulative unfolding probability, obtained by integrating and normalizing the unfolding force histograms of Fig. 3 *B* and Fig. 4 *B* is shown in Fig. 5. Remarkably, at 40 pN, 80% of ligand-less DHFR have already unfolded (*thick line* in Fig. 5), whereas only <10% of DHFR have unfolded in the presence of 190 μM MTX (*dashed line* in Fig. 5). These results show that upon binding MTX, the DHFR protein becomes mechanically stable.

DHF and NADPH ligands mechanically stabilize DHFR

The natural substrate DHF binds to DHFR at the same site as MTX, but the dissociation constant of human DHFR-DHF

TABLE 2 Mechanical properties of (DHFR-I27)$_4$ under various conditions

	F_u (DHFR) pN	ΔL_c (DHFR) nm	n	F_u (I27) pN	ΔL_c (I27) nm	n
No substrate	27	67*	163	209 $\pm$ 34	28.1 $\pm$ 1.3	226
19 μM MTX	74 $\pm$ 12	67.7 $\pm$ 0.5	95	193 $\pm$ 18	28.3 $\pm$ 0.7	67
190 μM MTX	82 $\pm$ 18	67.4 $\pm$ 1.0	277	220 $\pm$ 36	28.0 $\pm$ 0.7	322
1.2 mM MTX	77 $\pm$ 15	67.3 $\pm$ 0.5	66	194 $\pm$ 19	28.4 $\pm$ 1.8	96
180 μM DHF	83 $\pm$ 16	67.2 $\pm$ 1.1	36	212 $\pm$ 27	27.5 $\pm$ 0.2	32
210 μM NADPH	98 $\pm$ 15	67.4 $\pm$ 0.7	86	224 $\pm$ 29	27.8 $\pm$ 0.8	55
190 μM MTX 210 μM NADPH	83 $\pm$ 13	67.3 $\pm$ 0.8	136	190 $\pm$ 22	27.8 $\pm$ 0.7	120

*Assumed to be 67 nm to measure the unfolding forces.

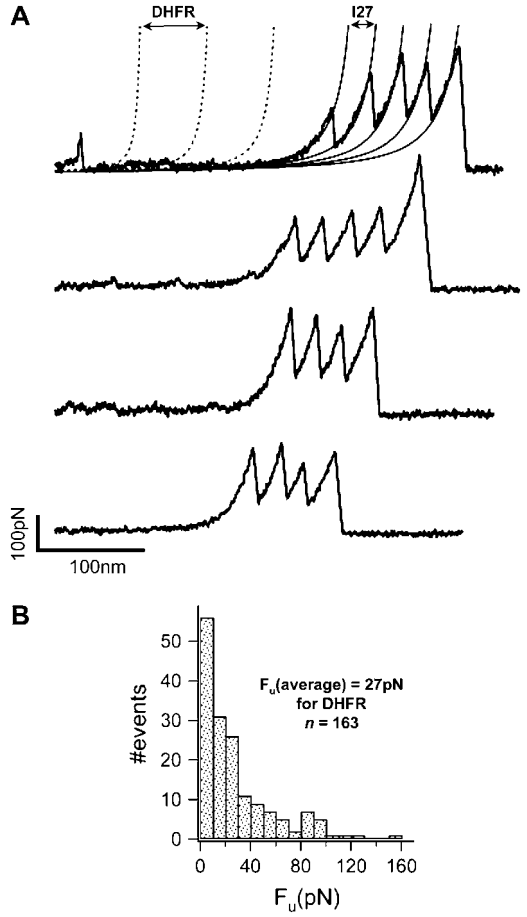

FIGURE 4 The mechanical stability of DHFR can be unambiguously determined using the $(DHFR\text{-}I27)_4$ polyprotein chimera. (*A*) A panel of four force-extension curves obtained by stretching $(DHFR\text{-}I27)_4$ in the absence of added MTX. The principal feature of these recordings is the long featureless spacer that we observe preceding the I27 unfolding events. The long spacer is marked occasionally by some low level unfolding peaks. By contrast, the I27 unfolding events can be readily observed and quantified with fits of the WLC (*thin lines*). The unfolding force of I27 is 209 ± 34 pN and the increment of contour length upon I27 unfolding is 28.1 ± 1.3 nm ($n = 226$). To estimate the force required to unfold DHFR, we generate a series of WLC curves, equally spaced by 67 nm (*dotted lines*), starting backward from the first I27 unfolding event. The intersection between these WLC curves and the experimental values are taken as the unfolding force for DHFR. (*B*) Histogram of the unfolding forces of DHFR. The mean unfolding force for DHFR is 27 pN ($n = 163$).

($K_d \approx 580$ nM) (41) is almost two orders-of-magnitude larger than the dissociation constant of DHFR-MTX (K_d <10 nM) (42). The mechanical properties of DHFR in the presence of 180 μM DHF are given in Table 2. The force required to unfold DHFR-DHF is 83 ± 16 pN ($n = 36$), which is similar to that of DHFR-MTX. In these experiments, the ligand concentration (180–190 μM) was always higher than the concentration of DHFR (~1 μM). Under these conditions, most of the DHFR (>99%) is in ligand-bound form and >99% of the binding sites of DHFR molecules are occupied.

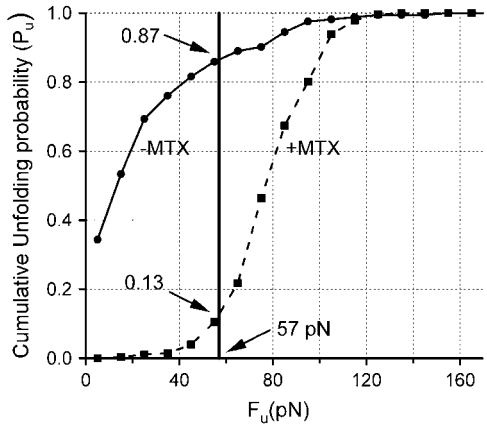

FIGURE 5 Plot of the cumulative unfolding probability as a function of unfolding force in the presence and absence of MTX at a constant pulling rate of 400 nm/s and a constant unfolding rate of ~6/s. The cumulative probability of unfolding was calculated by integrating the histograms of Fig. 3 *B* (+MTX) and Fig. 4 *B* (−MTX), and then normalizing them to 1. The thick vertical line marks a pulling force of 57 pN (see text). At this pulling force DHFR is most likely to be unfolded ($P_u = 0.87$). By contrast, the DHFR-MTX complex is most likely to remain folded ($P_u = 0.13$).

The coenzyme NADPH has a different binding site from MTX or DHF (1) with a dissociation constant of $K_d \approx 45$ nM (42). The unfolding force of DHFR in the presence of 210 μM NADPH is 98 ± 15 pN ($n = 86$), which is slightly larger than the rupture force obtained with MTX or DHF. However, this difference is within the margin of error of the measurement and may not be significant. Therefore, although MTX and NADPH bind at different sites in the protein, they induce similar mechanical stability in DHFR.

Interestingly, we found that MTX and NADPH were not additive in their stabilizing effects. We measured the force required to unfold DHFR in the presence of 190 μM MTX and 210 μM NADPH (Fig. 6). The figure shows that DHFR in the presence of both NADPH and MTX still requires 83 ± 13 pN ($n = 136$) to unfold, which is similar to the force required to unfold the DHFR-MTX complex or the DHFR-NADPH complex (Table 2). Despite the fact that the binding of MTX and NADPH to DHFR is cooperative (43), no additional mechanical stability was found when DHFR was occupied by both ligands simultaneously.

DISCUSSION

Mechanism of DHFR stabilization by MTX, DHF, and NADPH

A ligand (MTX, DHF, or NADPH) may stabilize DHFR against mechanical unfolding by several plausible general mechanisms. The increased mechanical stability could be the result of ligand-protein specific interactions, conformational changes triggered by ligand binding.

Ligand binding could introduce specific DHFR-ligand interactions, such as hydrogen bonds or van der Waals interactions, and these interactions contribute to directly resisting

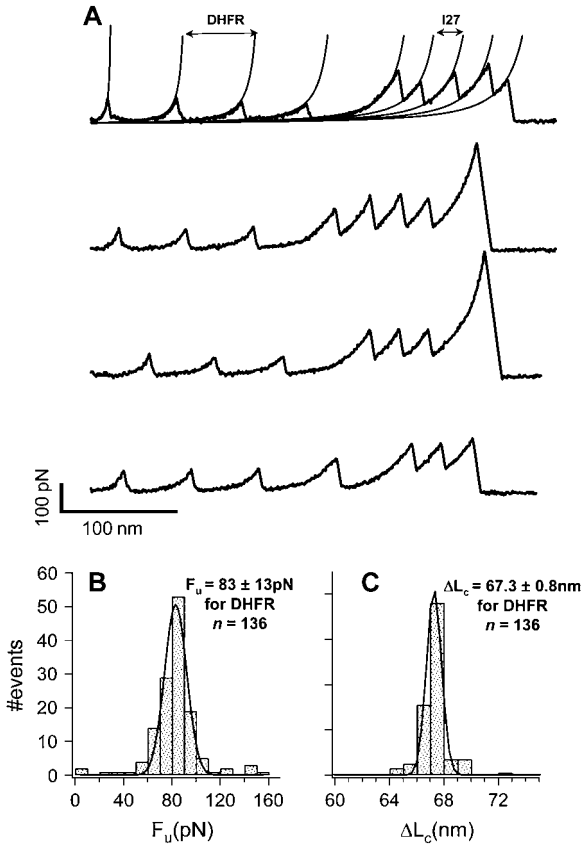

FIGURE 6 The mechanical stability of DHFR-MTX complex is not increased by adding a second ligand. (*A*) A panel of force-extension curves measured by stretching the $(DHFR\text{-}I27)_4$ polyprotein chimera in the presence of 190 μM MTX and 210 μM NADPH. Despite the fact that both MTX and NADPH stabilize DHFR to a similar extent (see Table 2), their stabilizing effects are not additive. As before, we measure the magnitude of the unfolding peaks for both DHFR and the I27 fingerprint (see Table 2). The thin lines are WLC fits. (*B*) Histogram of unfolding forces of DHFR in the presence of MTX and NADPH. A Gaussian fit (*thin line*) gives an unfolding force of 83 ± 13 pN ($n = 136$). (*C*) Histogram of contour length increments after DHFR unfolding measured with the WLC. A Gaussian fit (*thin line*) gives 67.3 ± 0.8 nm ($n = 136$). These results are indistinguishable from those obtained with either MTX or NADPH alone, indicating that their effect on the mechanical stability of DHFR is not additive.

the applied mechanical force. In such case, we expect a one-to-one relationship between binding strength and mechanical resistance. However, we can clearly rule this out, given that the force required to unfold the DHFR-MTX complex is the same as that required to unfold the DHFR-DHF complex, and that the dissociation constant of DHFR-MTX is >50-fold smaller than that of DHFR-DHF (<10 vs. 580 nM, see above). Similarly, the addition of a second ligand fails to increase the force required to unfold the DHFR complex.

Ligand binding could cause a conformational change in DHFR, thereby bringing the protein into a mechanically stable state. It is already known that ligand binding induces conformational changes in the DHFR molecule (44). Studies of the crystal structure of *Escherichia coli* DHFR before and after binding a ligand show large conformational changes in the Met20, G-H, and F-G loops (44). These extensive conformational rearrangements upon binding different ligands suggest that the flexibility of DHFR is modulated by ligand binding. It has been speculated that the structural fluctuations observed in *E. coli* DHFR are necessary to accommodate the intermediates that form during the catalytic cycle (44). Using hydrogen/deuterium exchange to probe the amplitude of these fluctuations Yamamoto and colleagues (45) found that the binding of either folate or NADPH reduced hydrogen/deuterium exchange, indicating that the structural fluctuations of DHFR were reduced by ligand binding. Furthermore, they found that the magnitude of the reduction in the amplitude of the fluctuations was not additive, when both folate and NADPH were simultaneously bound to DHFR (45). It is tempting to conclude that the fluctuations in the *E. coli* DHFR structure, as well as their reduction in the presence of ligands, are correlated with the changes in mechanical stability that we observe in our single-molecule AFM studies. However, since the CHO-DHFR used in our studies is <30% homologous to its bacterial counterpart, it may be misleading to compare the DHFRs from the two species. Instead, it should be more appropriate to compare the CHO-DHFR with the human version, because the protein sequences are 90% identical. In urea denaturation, human DHFR is only marginally stable in the absence of ligands, with $\Delta G_{\text{U-N}} = 2.4$ kcal/mol (9). Binding of folate and $NADP^+$ stabilize human DHFR by ≈3.5 kcal/mol (9). High concentrations of human apo-DHFR have a strong tendency to aggregate (9), and human DHFR has been crystallized only when it is bound to ligands (4).

DHFR translocation across the mitochondrial membrane

Nearly two decades ago, Eiler and Schatz (10) demonstrated that MTX blocks the translocation of DHFR through the mitochondrial membrane by preventing the unfolding of the protein. Since then, MTX-bound DHFR has served as the benchmark molecule in protein translocation across mitochondrial membrane, as well as in protein degradation by ATP-dependent proteases. It is widely believed that, to fit into the narrow translocation or degradation channel, at least a portion of the folded protein must be converted to a threadlike conformation (14–16,46,47). However, there is little consensus on how this conversion occurs. Our single-molecule results show conclusively that ligand binding stabilizes DHFR mechanically. Therefore, if the rate-determining step in protein translocation were the force-induced unraveling of a protein, then our results would explain why the MTX-DHFR complex is resistant to translocation.

DHFR degradation by the proteasome

The significance of the finding that the mechanical stability of DHFR is dependent on ligand binding is best illustrated

when considering proteasomal degradation. The proteasome degrades ubiquitin-tagged DHFR at a rate $\sim 0.05\ \mathrm{min}^{-1}$ (12,23). In these experiments it was clearly established that the rate-limiting step was the unfolding of DHFR (23). Furthermore, as it had been shown earlier for translocation of DHFR across the mitochondrial membrane, addition of MTX reduced the rate of degradation by >10-fold (12,23). It has been recently proposed that a mechanical force generated by the proteasomal ATPase motor triggers the unfolding of the targeted protein (12,48). This model is equivalent to a medieval rack, where the ATPase motor pulls on DHFR against a ubiquitin chain bound to the proteasome, until DHFR unfolds. This model predicts that there should be a close correlation between the effect of MTX on the proteasomal degradation of DHFR, and its mechanical stability.

In our experiments, we pull the $(\text{DHFR-I27})_4$ polyprotein at a constant rate. The DHFR unfolding rate α_u, at a given pulling force F, can be modeled as

$$\alpha_u = \alpha_{F=0} \cdot e^{\frac{F\cdot\Delta x}{kT}},$$

where k is the Boltzmann constant, T is the absolute temperature, and Δx is the distance from the folded state to the transition state in the direction of the reaction coordinate. In the presence of ligands, DHFR has a distinct mechanical fingerprint, and its average unfolding force increases from 62 pN at 80 nm/s to 80 pN at 400 nm/s. Through fits to Monte Carlo simulations (28,49) we estimated a value of $\Delta x = 0.37$ nm. To compare the unfolding rates of DHFR in the presence and absence of ligands, we assume that Δx is unchanged by ligand binding. However, this assumption remains untested, given that we cannot accurately measure the unfolding force for DHFR in the absence of ligands at any pulling rate.

Given that all DHFR molecules contained in a polyprotein are forced to unfold during the time of an experiment (e.g., see Fig. 3 *A* and Fig. 4 *A*), the observed unfolding rate is constant, and independent of whether MTX was present or not. However, the force, required to unfold within that time, was strongly dependent on the presence of MTX. Thus, we can then write

$$\frac{\alpha_u^{-\mathrm{MTX}}}{\alpha_u^{+\mathrm{MTX}}} = 1 = \frac{\alpha_{F=0}^{-\mathrm{MTX}} \cdot e^{\frac{27*0.37}{kT}}}{\alpha_{F=0}^{+\mathrm{MTX}} \cdot e^{\frac{80*0.37}{kT}}}.$$

Solving this equation, we obtain

$$\alpha_{F=0}^{-\mathrm{MTX}} = 120 \cdot \alpha_{F=0}^{+\mathrm{MTX}}.$$

Hence, our results on the effect of MTX on the mechanical stability of DHFR predict that the unfolding rate of DHFR is 120-times bigger than that of the DHFR-MTX complex. This will remain true for unfolding rates compared at any pulling force. This estimate agrees with the independently measured degradation half-lives of DHFR and DHFR-MTX complex in the proteasome (12,23). Therefore, force-induced unfolding is certainly a plausible mechanism in proteasomal degradation.

The proteasomal motor is an AAA ATPase. The AAA ATPases are ringlike hexameric motor proteins that are thought to convert conformational changes of the ring into a pulling force along a linear processive motion (50). Although there are no direct measurements of the mechanical capacity of the proteasomal motor, we use, as a model, the bacteriophage portal motor—a similar ringlike ATPase that also converts conformational changes of its ring into a linear translocation, and is capable of generating average forces of 57 pN (51). Fig. 5 shows the change in the cumulative unfolding probability of DHFR, triggered by the binding of MTX. At 57 pN, DHFR will be mostly unfolded ($P_u = 0.87$), whereas the DHFR-MTX complex will remain mostly folded ($P_u = 0.13$). It is interesting to note that the widest gap in the plot of Fig. 5 occurs precisely around the range of forces known to be generated by an AAA ATPase motor.

We thank Dr. Hongbin Li and Dr. Atom Sarkar for stimulating discussions.

The Chinese hamster DHFR gene is a generous gift from Professor L. A. Chasin. This work has been supported by National Institutes of Health grants to J.M.F. L.L. is a Damon Runyon Fellow (DRG-No. 1792-03).

REFERENCES

1. Schnell, J. R., H. J. Dyson, and P. E. Wright. 2004. Structure, dynamics, and catalytic function of dihydrofolate reductase. *Annu. Rev. Biophys. Biomol. Struct.* 33:119–140.
2. Benkovic, S. J., and S. Hammes-Schiffer. 2003. A perspective on enzyme catalysis. *Science*. 301:1196–1202.
3. Pineda, P., A. Kanter, R. S. McIvor, S. J. Benkovic, A. Rosowsky, and C. R. Wagner. 2003. Dihydrofolate reductase mutant with exceptional resistance to methotrexate but not to trimetrexate. *J. Med. Chem.* 46: 2816–2818.
4. Davies, J. F., T. J. Delcamp, N. J. Prendergast, V. A. Ashford, J. H. Freisheim, and J. Kraut. 1990. Crystal structures of recombinant human dihydrofolate reductase complexed with folate and 5-deazafolate. *Biochemistry*. 29:9467–9479.
5. Focia, P. J., I. V. Shepotinovskaya, J. A. Seidler, and D. M. Freymann. 2004. Heterodimeric GTPase core of the SRP targeting complex. *Science*. 303:373–377.
6. Bouzat, C., F. Gumilar, G. Spitzmaul, H.-L. Wang, D. Rayes, S. B. Hansen, P. Taylor, and S. M. Sine. 2004. Coupling of agonist binding to channel gating in an ACh-binding protein linked to an ion channel. *Nature*. 430:896–900.
7. Yamniuk, A. P., L. T. Nguyen, T. T. Hoang, and H. J. Vogel. 2004. Metal ion binding properties and conformational states of calcium- and integrin-binding protein. *Biochemistry*. 43:2558–2568.
8. Brzeska, H., S. V. Venyaminov, Z. Gravarek, and W. Drabikowski. 1983. Comparative studies on thermostability of calmodulin, skeletal muscle troponin C and their triptic fragments. *FEBS Lett.* 153:169–173.
9. Wallace, L. A., and C. R. Matthews. 2002. Highly divergent dihydrofolate reductases conserve complex folding mechanisms. *J. Mol. Biol*. 315:193–211.
10. Eilers, M., and G. Schatz. 1986. Binding of a specific ligand inhibits import of a purified precursor protein into mitochondria. *Nature*. 322:228–232.
11. Matouschek, A., N. Pfanner, and W. Voos. 2000. Protein unfolding by mitochondria. The Hsp70 import motor. *EMBO J*. 1:404–410.
12. Lee, C., M. P. Schwartz, S. Prakash, M. Iwakura, and A. Matouschek. 2001. ATP-dependent proteases degrade their substrates by processively

unraveling them from the degradation signal. *Mol. Cell.* 7: 627–637.

13. Prakash, S., L. Tian, K. S. Ratliff, R. E. Lehotzky, and A. Matouschek. 2004. An unstructured initiation site is required for efficient proteasome-mediated degradation. *Nat. Struct. Mol. Biol.* 11:830–837.
14. Hill, K., K. Model, M. T. Ryan, K. Dietmeier, F. Martin, R. Wagner, and N. Pfanner. 1998. Tom40 forms the hydrophilic channel of the mitochondrial import pore for preproteins. *Nature.* 395:516–521 [see comment].
15. Kunekle, K. P., S. Heins, M. Dembowski, F. E. Nargang, R. Benz, M. Thieffry, J. Walz, R. Lill, S. Nussberger, and W. Neupert. 1998. The preprotein translocation channel of the outer membrane of mitochondria. *Cell.* 93:1009–1019.
16. Okamoto, K., A. Brinker, S. A. Paschen, I. Moarefi, M. Hayer-Hartl, W. Neupert, and M. Brunner. 2002. The protein import motor of mitochondria: a targeted molecular ratchet driving unfolding and translocation. *EMBO J.* 21:3659–3671.
17. Prakash, S., and A. Matouschek. 2004. Protein unfolding in the cell. *Trends Biochem. Sci.* 29:593–600.
18. Sauer, R. T., D. N. Bolon, B. M. Burton, R. E. Burton, J. M. Flynn, R. A. Grant, G. L. Hersch, S. A. Joshi, J. A. Kenniston, I. Levchenko, S. B. Neher, E. S. Oakes, S. M. Siddiqui, D. A. Wah, and T. A. Baker. 2004. Sculpting the proteome with AAA^+ proteases and disassembly machines. *Cell.* 119:9–18.
19. Matouschek, A. 2003. Protein unfolding—an important process in vivo? *Curr. Opin. Struct. Biol.* 13:98–109.
20. Kenniston, J. A., T. A. Baker, and R. T. Sauer. 2005. Partitioning between unfolding and release of native domains during ClpXP degradation determines substrate selectivity and partial processing. *Proc. Natl. Acad. Sci. USA.* 102:1390–1395.
21. Huang, S., K. S. Ratliff, M. P. Schwartz, J. M. Spenner, and A. Matouschek. 1999. Mitochondria unfold precursor proteins by unraveling them from their N-termini. *Nat. Struct. Biol.* 6:1132–1138.
22. Matouschek, A., A. Azem, K. Ratliff, B. S. Glick, K. Schmid, and G. Schatz. 1997. Active unfolding of precursor proteins during mitochondrial protein import. *EMBO J.* 16:6727–6736.
23. Thrower, J. S., L. Hoffman, M. Rechsteiner, and C. M. Pickart. 2000. Recognition of the polyubiquitin proteolytic signal. *EMBO J.* 19:94–102.
24. Fisher, T. E., A. F. Oberhauser, M. Carrion-Vazquez, P. E. Marszalek, and J. M. Fernandez. 1999. The study of protein mechanics with the atomic force microscope. *Trends Biochem. Sci.* 24:379–384.
25. Carrion-Vazquez, M., A. F. Oberhauser, T. E. Fisher, P. E. Marszalek, H. Li, and J. M. Fernandez. 2000. Mechanical design of proteins studied by single-molecule force spectroscopy and protein engineering. *Prog. Biophys. Mol. Biol.* 74:63–91.
26. Rief, M., M. Gautel, F. Oesterhelt, J. M. Fernandez, and H. E. Gaub. 1997. Reversible unfolding of individual titin immunoglobulin domains by AFM. *Science.* 276:1109–1112.
27. Marszalek, P. E., H. Lu, H. Li, M. Carrion-Vazquez, A. F. Oberhauser, K. Schulten, and J. M. Fernandez. 1999. Mechanical unfolding intermediates in titin modules. *Nature.* 402:100–103.
28. Carrion-Vazquez, M., A. F. Oberhauser, S. B. Fowler, P. E. Marszalek, S. E. Broedel, J. Clarke, and J. M. Fernandez. 1999. Mechanical and chemical unfolding of a single protein: a comparison. *Proc. Natl. Acad. Sci. USA.* 96:3694–3699.
29. Li, H., A. F. Oberhauser, S. B. Fowler, J. Clarke, and J. M. Fernandez. 2000. Atomic force microscopy reveals the mechanical design of a modular protein. *Proc. Natl. Acad. Sci. USA.* 97:6527–6531.
30. Kenniston, J. A., T. A. Baker, J. M. Fernandez, and R. T. Sauer. 2003. Linkage between ATP consumption and mechanical unfolding during the protein processing reactions of an AAA^+ degradation machine. *Cell.* 114:511–520.
31. Carrion-Vazquez, M., H. Li, H. Lu, P. E. Marszalek, A. F. Oberhauser, and J. M. Fernandez. 2003. The mechanical stability of ubiquitin is linkage-dependent. *Nat. Struct. Biol.* 10:738–743.
32. Brockwell, D. J., E. Paci, R. C. Zinober, G. S. Beddard, P. D. Olmsted, D. A. Smith, R. N. Perham, and S. E. Radford. 2003. Pulling geometry defines the mechanical resistance of a β-sheet protein. *Nat. Struct. Biol.* 10:731–737.
33. Oberhauser, A. F., P. E. Marszalek, H. P. Erickson, and J. M. Fernandez. 1998. The molecular elasticity of the extracellular matrix protein tenascin. *Nature.* 393:181–185.
34. Florin, E. L., M. Rief, H. Lehmann, M. Ludwig, K. Dornmair, V. T. Moy, and H. E. Gaub. 1995. Sensing specific molecular interactions with the atomic force microscope. *Biosens. Bioelectron.* 10:895–901.
35. Carrion-Vazquez, M., P. E. Marszalek, A. F. Oberhauser, and J. M. Fernandez. 1999. Atomic force microscopy captures length phenotypes in single proteins. *Proc. Natl. Acad. Sci. USA.* 96:11288–11292.
36. Fisher, T. E., P. E. Marszalek, and J. M. Fernandez. 2000. Stretching single molecules into novel conformations using the atomic force microscope. *Nat. Struct. Biol.* 7:719–724.
37. Li, H., A. F. Oberhauser, S. D. Redick, M. Carrion-Vazquez, H. P. Erickson, and J. M. Fernandez. 2001. Multiple conformations of PEVK proteins detected by single-molecule techniques. *Proc. Natl. Acad. Sci. USA.* 98:10682–10686.
38. Best, R. B., B. Li, A. Steward, V. Daggett, and J. Clarke. 2001. Can non-mechanical proteins withstand force? Stretching barnase by atomic force microscopy and molecular dynamics simulation. *Biophys. J.* 81: 2344–2356.
39. Endo, T., and G. Schatz. 1988. Latent membrane perturbation activity of a mitochondrial precursor protein is exposed by unfolding. *EMBO J.* 7:1153–1158.
40. Atreya, C. E., and K. S. Anderson. 2004. Kinetic characterization of bifunctional thymidylate synthase-dihydrofolate reductase (TS-DHFR) from *Cryptosporidium hominis*: a paradigm shift for TS activity and channeling behavior. *J. Biol. Chem.* 279:18314–18322.
41. Tsay, J.-T., J. R. Appleman, W. A. Beard, N. J. Prendergast, T. J. Delcamp, J. H. Freisheim, and R. L. Blakley. 1990. Kinetic investigation of the functional role of phenylalanine-31 of recombinant human dihydrofolate reductase. *Biochemistry.* 29:6428–6436.
42. Appleman, J. R., N. Prendergast, T. J. Delcamp, J. H. Freisheim, and R. L. Blakley. 1988. Kinetics of the formation and isomerization of methotrexate complexes of recombinant human dihydrofolate reductase. *J. Biol. Chem.* 263:10304–10313.
43. Bystroff, C., and J. Kraut. 1991. Crystal structure of unliganded *Escherichia coli* dihydrofolate reductase. Ligand-induced conformational changes and cooperativity in binding. *Biochemistry.* 30:2227–2239.
44. Sawaya, M. R., and J. Kraut. 1997. Loop and subdomain movements in the mechanism of *Escherichia coli* dihydrofolate reductase: crystallographic evidence. *Biochemistry.* 36:586–603.
45. Yamamoto, T., S. Izumi, and K. Gekko. 2004. Mass spectrometry on hydrogen/deuterium exchange of dihydrofolate reductase: effects of ligand binding. *J. Biochem.* (*Tokyo*). 135:663–671.
46. Larsen, C. N., and D. Finley. 1997. Protein translocation channels in the proteasome and other proteases. *Cell.* 91:431–434.
47. Horwich, A. L., E. U. Weber-Ban, and D. Finley. 1999. Chaperone rings in protein folding and degradation. *Proc. Natl. Acad. Sci. USA.* 96:11033–11040.
48. Hochstrasser, M., and J. Wang. 2001. Unraveling the means to the end in ATP-dependent proteases. *Nat. Struct. Biol.* 8:294–296.
49. Rief, M., J. M. Fernandez, and H. E. Gaub. 1998. Elastically coupled two-level systems as a model for biopolymer extensibility. *Phys. Rev. Lett.* 81:4764–4767.
50. Vale, R. D. 2000. AAA proteins. Lords of the ring. *J. Cell Biol.* 150:F13–F19.
51. Smith, D. E., S. J. Tans, S. B. Smith, S. Grimes, D. L. Anderson, and C. Bustamante. 2001. The bacteriophage straight φ29 portal motor can package DNA against a large internal force. *Nature.* 413:748–752.